JMEPEG
DOI: 10.1007/s11665-016-2236-8

©ASM International
1059-9495/$19.00

Numerical and Experimental Study on the Residual Stresses in the Nitrided Steel

X. Song, Zhi-Qian Zhang, S. Narayanaswamy, Y.Z. Huang, and M. Zarinejad

(Submitted November 23, 2015; in revised form June 24, 2016)

In the present work, residual stresses distribution in the gas nitrided AISI 4140 sample has been studied using finite element (FE) simulation. The nitrogen concentration profile is obtained from the diffusion-controlled compound layer growth model, and nitrogen concentration controls the material volume change through phase transformation and lattice interstitials which results in residual stresses. Such model is validated through residual stress measurement technique—micro-ring-core method, which is applied to the nitriding process to obtain the residual stresses profiles in both the compound and diffusion layer. The numerical and experimental results are in good agreement with each other; they both indicate significant stress variation in the compound layer, which was not captured in previous research works due to the resolution limit of the traditional methods.

Keywords digital image correlation (DIC), finite element (FE), focused ion beam (FIB), gas nitriding, residual stresses

1. Introduction

Gas nitriding is a process of case hardening in which a ferrous alloy, usually of special composition, is heated in an atmosphere of ammonia to produce surface hardening by absorption of nitrogen, without quenching (Ref 1). It leads to various types of mechanical property enhancement, such as hardness increment and fatigue life improvement, and hence is widely used in aerospace and automotive industries. Comparing with carburization, nitriding requires neither high-temperature processing nor severe quenching process; hence, no significant dimensional change is involved and less distortion is observed. Therefore, nitriding has been widely considered as an important surface treatment method for near-net-shape processing of high-value-added components.

A typical gas nitrided case consists of two zones. The outer zone, which is called "compound layer" or "white layer," consists predominately of ε-Fe_{2-3}(C, N) and/or γ′-Fe_4N. It is usually very hard and brittle, but highly resistant to wear and corrosion (Ref 2). It remains on the immediate steel surface and becomes thicker with gas concentration, time, and temperature. The zone beneath the compound layer is known as diffusion zone. For pure iron, in the diffusion zone, nitrogen dissolves interstitially in ferric lattice at nitriding temperature. For steel with tempered martensite (Fe_3C + ferric together with other carbides), the nitrogen not only dissolves interstitially in ferric but also reacts with carbides to form carbon nitrides (Ref 3). For steels that contain nitride-forming elements (e.g., AISI 4140), alloy nitrides will be formed within diffusion zone (Ref 4). The hardened diffusion zone is responsible for a considerable enhancement of the fatigue endurance due to the introduction of compressive residual stress during nitriding.

The effort to understand the nitriding process through numerical simulation has been ongoing for the last 20 years. Most of the successful works are in the area of simulating the nitriding process of pure iron (Ref 5, 6). Good agreement has been achieved by using various diffusion models. However, the simulations in steels become more complicated, since the well-defined ε and γ′ sub-layers in nitrided pure iron are replaced by the mixture of these two phases in nitrided steel. Recently, the layer growth model has been developed to simulate the layer growth kinetics for nitriding AISI 4140 steel based on the customized Lehrer diagram (Ref 7). This model can be used to calculate concentration profiles of nitrogen as a function of time and position during the nitriding process. However, such model has not been extended to the application of residual stresses estimation during nitriding, whereas residual stresses are widely considered to have direct link with component dimensional accuracy (distortion) and fatigue life.

In gaseous nitriding, the residual stresses are originally from the modification of chemical composition and crystal structure by precipitation inside diffusion layer. The surface hardness has been extensively studied for nitriding process. However, only a limited number of papers deal with the measurement of residual stresses in nitriding and related technologies (Ref 8-11). The reason may be that nitriding suffers less distortion and lower residual stresses comparing with carburizing. In addition, most data in the literature are relevant to residual stress in diffusion zone; it is rare to find those for the compound layer (Ref 8). However, for precision engineering applications, when the compound layer thickness is comparable to total case thickness or even to the component characteristic dimension, the influence of the residual stresses in the compound layer could be significant.

Data in the literature show a wide range of values for residual stresses. Initial investigations have shown that

X. Song and **M. Zarinejad**, Singapore Institute of Manufacturing Technology (SIMTech), A*STAR, Singapore 637662, Singapore; **Zhi-Qian Zhang** and **S. Narayanaswamy**, Institute of High Performance Computing (IHPC), A*STAR, Singapore 138632, Singapore; and **Y.Z. Huang**, School of Materials Science and Engineering, Nanyang Technological University, Singapore 639798, Singapore. Contact e-mail: songx02@gmail.com.

Published online: 20 July 2016

compressive residual stresses exist in compound layer during layer growth and the stresses increase during cooling as consequence of different thermal expansion coefficients of compound layer and diffusion zone which generate volume misfit (Ref 9). Further studies have shown that tensile stresses appear in ε compound layers and compressive stresses appear in γ′ compound layers (Ref 8). All the available data indicate that higher compressive stresses exist in compound layers of pure γ′ comparing with those in ε or ε + γ′ layer. The carbon content of substrate has a considerable effect on residual stresses, as increased carbon content results in increased residual stress level (Ref 9). The significance of carbon content is more obvious in ε-$Fe_{2\text{-}3}N$ structures, which is due to the increased solubility of carbon in compact hexagonal ε-$Fe_{2\text{-}3}N$ crystals. Previous investigations have shown that compressive stresses appear in compound layer due to volume changes during ε-crystal formation as a result of dissolved carbon from the matrix (Ref 8). Due to the solubility of carbon in ε-nitrides (carbonitrides), the carbide particles of the pearlite grains in the interface are dissolved in ε-crystals. Thus, the compound layer is "rooting" in the substrate at the boundaries of pearlite grains, which causes compressive residual stresses not only in compound layer, but also in substrate in interface region.

For measuring the residual stresses on the surface, two distinctive classes of techniques are commonly used: destructive and nondestructive methods. The most prominent and versatile nondestructive method is x-ray diffraction. In thin solid film applications, $\sin^2\psi$ method is often used (Ref 12) due to its near-surface nature, but its application is generally limited to the crystalline materials (Ref 13). Moreover, the $\sin^2\psi$ method, based on the assumption of plane stress condition, is not always valid. In fact, the residual stress value obtained by this method is actually an average value over the x-ray penetration depth, i.e., for 8 keV x-ray source with Fe sample, the 90% attenuation depth is around 10 μm, which means the residual stress value it obtains is an average value over 10 μm depths. This is the actual resolution for the x-ray diffraction method if small depth increment is used rather than resolution of the electro-polishing material removal step. Therefore, such method may work for relatively thick films of >50 μm, but for thin films of 10-20 μm (typical nitriding component layer thickness), it may not be accurate enough to obtain the stress variation in the film in the depth direction. The destructive method, on the other hand, is applicable to a wider range of materials and independent of scale. It relies on monitoring the local component geometry changes, either in the process of residual stress introduction, or subsequent relaxation, e.g., due to mechanical or electrochemical removal of material. Common destructive methods include hole drilling, crack compliance, and curvature measurement (Ref 14). These methods can be easily adopted in the micro- to nano-scopic level (Ref 15) by using micro- and nano-machining tool, notably focused ion beam (FIB). Korsunsky et al. (Ref 13, 16, 17), Kang (Ref 18) and Krottenthaler (Ref 19) have carried out extensive research on the residual stresses measurement at microscale using dual beam system (SEM+FIB). Effort to employ single instrument FIB for both imaging and milling has also been made (Ref 20). In the current study, we employ the dual beam system (SEM+FIB), for its high measurement precision to obtain the residual stresses in the nitrided component, in both the compound and diffusion layer. This result is used to validate the compound layer growth model we have employed in the finite element (FE) simulation to predict the residual stresses and distortion in the nitriding of AISI 4140 sample. The numerical and experimental results show good agreement with each other, indicating a significant stress variation in the compound layer, which was not able to be captured in previous studies due to the resolution limit.

2. The Finite Element Simulation

The residual strains and stresses of the nitrided AISI 4140 steel components result from the diffusion of nitrogen into the specimen from the surface. Due to the different concentrations of nitrogen, the nitrided AISI 4140 steel components will form different layers, such as compound layer and diffusion zone (Ref 4). The diffusion of nitrogen atoms will lead to the volume change in the matrix lattice. The concentration of nitrogen varies with respect to the different depth from the surface and consequently introduces the varying residual stress fields. The concentration profile of nitrogen is highly influenced by many nitriding operational conditions, such as nitrogen concentration at the surface and the nitriding time. To analyze the influence of the nitriding operational conditions on the nitriding effects, trial and error can always be used to determine the parameters so as to meet the specifications. However, this method is time-consuming and hard to control. Therefore, an effective simulation tool is needed to simulate the nitriding process, which is able to examine the nitriding operational conditions and estimate the residual stresses. In this section, a model for estimating the residual strain related to nitrogen concentration has been introduced, and a numerical simulation tool for nitriding process on AISI 4140 steel is developed based on the commercial finite element software package ABAQUS™.

2.1 Nitrogen Concentration Profile

The concentration profile of the nitrogen is determined by the nitrogen diffusion, which can be described by the compound layer growth model (Ref 4, 21). The compound layer growth model for nitriding AISI 4140 is developed based on the customized Lehrer diagram, which can be used to calculate the concentration profile of nitrogen as a function of time and position. Comparing the dimension of the nitrided specimen, the maximum depth which the nitrogen diffusion can reach is small, and therefore, the three-dimensional nitrogen diffusion problem can be simplified as a semi-infinite diffusion model along the inner surface normal direction as shown in Fig. 1, which can be described by a compound layer growth model (Ref 4, 21). In this model, there is a moving interface between the compound layer and the diffusion zone, as shown in Fig. 1, where the local coordinate axis ox direction denotes the inner surface normal direction.

In the present paper, c denotes the concentration of nitrogen. c_c and c_d denote the nitrogen concentration in the compound layer and the diffusion zone, respectively. The depth of the moving interface between compound layer and diffusion zone is defined by $x = \xi(t)$ at time t. N_s denotes the nitrogen concentration at the surface. N_c and N_d are the nitrogen concentration in compound layer and diffusion zone at the interface, respectively. N_s is determined by the operational conditions. N_c and N_d are two constants for AISI 4140 steel (Ref 4).

To find the nitrogen concentration profile, the semi-infinite diffusion problem can be governed by the following second

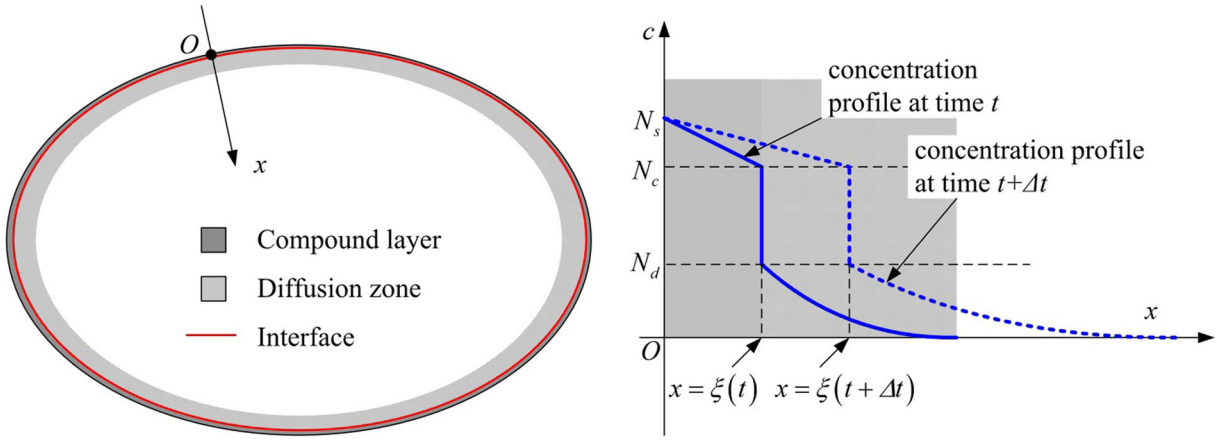

Fig. 1 Schematics of diffusion problem in nitriding process: (left) illustration of cross section of component being nitrided; (right) concentration profiles of nitrogen at different time

Fick's law with the corresponding boundary and initial conditions.

$$\begin{aligned} &\frac{\partial c_c}{\partial t} = D_c \frac{\partial^2 c_c}{\partial x^2}, \quad \text{in compoud layer } 0 \le x \le \xi(t). \\ &c_c = N_s, \quad \text{at } x = 0; \quad c_c = N_c, \quad \text{at } x = \xi(t). \\ &c_c = 0, \text{ at } t = 0. \end{aligned} \tag{Eq 1}$$

$$\begin{aligned} &\frac{\partial c_d}{\partial t} = D_d \frac{\partial^2 c_d}{\partial x^2}, \quad \text{in diffusion zone } x \ge \xi(t). \\ &c_d = N_d, \quad \text{at } x = \xi(t); \quad c_d = 0, \quad \text{at } x \to \infty. \\ &c_d = 0, \text{ at } t = 0. \end{aligned} \tag{Eq 2}$$

The key to solve this moving interface diffusion problem is to find the interface location $\xi(t)$ at time t, which has been theoretically solved previously (Ref 22). The location of the interface can be written in the following quadratic form

$$\xi(t) = k\sqrt{t}. \tag{Eq 3}$$

Here, the parameter k can be identified by the experimental data.

The analytical solutions of diffusion problem with moving interface defined by Eq 1 and 2 can be written as follows (Ref 21, 22),

$$\begin{aligned} c_c &= N_s + A\,\mathrm{erf}\left(x/\left(2\sqrt{D_c t}\right)\right), \quad 0 \le x \le \xi(t). \\ c_d &= N_d + B\,\mathrm{erf}\left((x-\xi(t))/\left(2\sqrt{D_d t}\right)\right), \quad x \ge \xi(t). \end{aligned} \tag{Eq 4}$$

where erf denotes the error function and D_c and D_d denote the diffusion coefficients in the compound layer and the diffusion zone, respectively. Imposing the boundary conditions into Eq 4, the parameters A and B can be solved, and the whole nitrogen concentration profile can be summarized as follows,

$$c = \begin{cases} N_s + \frac{N_c - N_s}{\mathrm{erf}\left(k/2\sqrt{D_c}\right)} \mathrm{erf}\left(\frac{x}{2\sqrt{D_c t}}\right) & 0 \le x \le k\sqrt{t} \\ N_d\left(1 - \mathrm{erf}\frac{x-\xi(t)}{2\sqrt{D_d t}}\right) & x \ge k\sqrt{t} \end{cases}. \tag{Eq 5}$$

In order to verify the solution in Eq 5, this method is used to solve the nitrogen concentration profile of nitriding process for AISI 4140 steel with the given parameters $N_s = 7.18$ wt.%, $N_c = 6.5$ wt.%, $N_d = 1.3$ wt.%, $D_c = 6.5 \times 10^{-14}\mathrm{m}^2/\mathrm{s}$, $D_d = 5 \times 10^{-13}\mathrm{m}^2/\mathrm{s}$, and $B = 4.3303 \times 10^{-8}\mathrm{m/s}^{1/2}$ (Ref 4). The parameter $k = 4.3303 \times 10^{-8}\mathrm{m/s}^{1/2}$ for locating moving interface is identified by experimental data (Ref 4), that is, thickness of compound layer is 20 μm after 60-h nitriding. The comparisons of nitrogen concentration profiles obtained by the experimental data, the reference numerical solutions (Ref 4), and the present method are illustrated in Fig. 2. The good agreement observed in Fig. 2 clearly validates the method proposed above. Using such solution, the nitrogen concentration profiles for different nitriding time can be readily obtained (Fig. 2).

2.2 Residual Volumetric Strain

During nitriding, the nitrogen atoms diffuse into the substrate and the non-uniform nitrogen concentration profile as modeled in section 2.1 will lead to chemical and microstructural gradient, which introduces heterogeneities at the microscopic scale. The resultant microscopic heterogeneities bring about the heterogeneities of the residual volume strain $\varepsilon_{ij}^{\mathrm{vol}}$, due to the structural dilation induced by nitrogen diffusion. As a consequence, the total residual strain ε_{ij}^{R} of nitriding arises from various sources, such as structure dilation $\varepsilon_{ij}^{\mathrm{vol}}$, thermal ε_{ij}^{T}, and plastic ε_{ij}^{p}, i.e., $\varepsilon_{ij}^{\mathrm{res}} = \varepsilon_{ij}^{\mathrm{vol}} + \varepsilon_{ij}^{p} + \varepsilon_{ij}^{T}$. The residual strain will cause the macroscopic residual stress σ_{ij}^{R} and hence yield the distortion of the component after nitriding. The plastic part ε_p and thermal part ε_T can be evaluated using the classical solid mechanics theory. However, the dilation part $\varepsilon_{ij}^{\mathrm{vol}}$ needs to be considered in the microscopic point of view.

The method proposed in (Ref 23-25) is employed in this research to calculate $\varepsilon_{ij}^{\mathrm{vol}}$. The method and only the key formulations are briefly reviewed in this paper for the sake of simplicity. The method is based on self-consistent scheme of n phases (ferrite and n-1 phases), which has been demonstrated in agreement with mechanical model of nitriding, as well as XRD analysis. The model is governed by the volume changes resulting from precipitation, which is measured by comparing the volume of precipitates at a given depth at two successive time steps (i.e., t and $t + \Delta t$). The specific volume v_{Φ_i} of the phase Φ_i and the volume of the participates V_P at a given temperature can be written as follows,

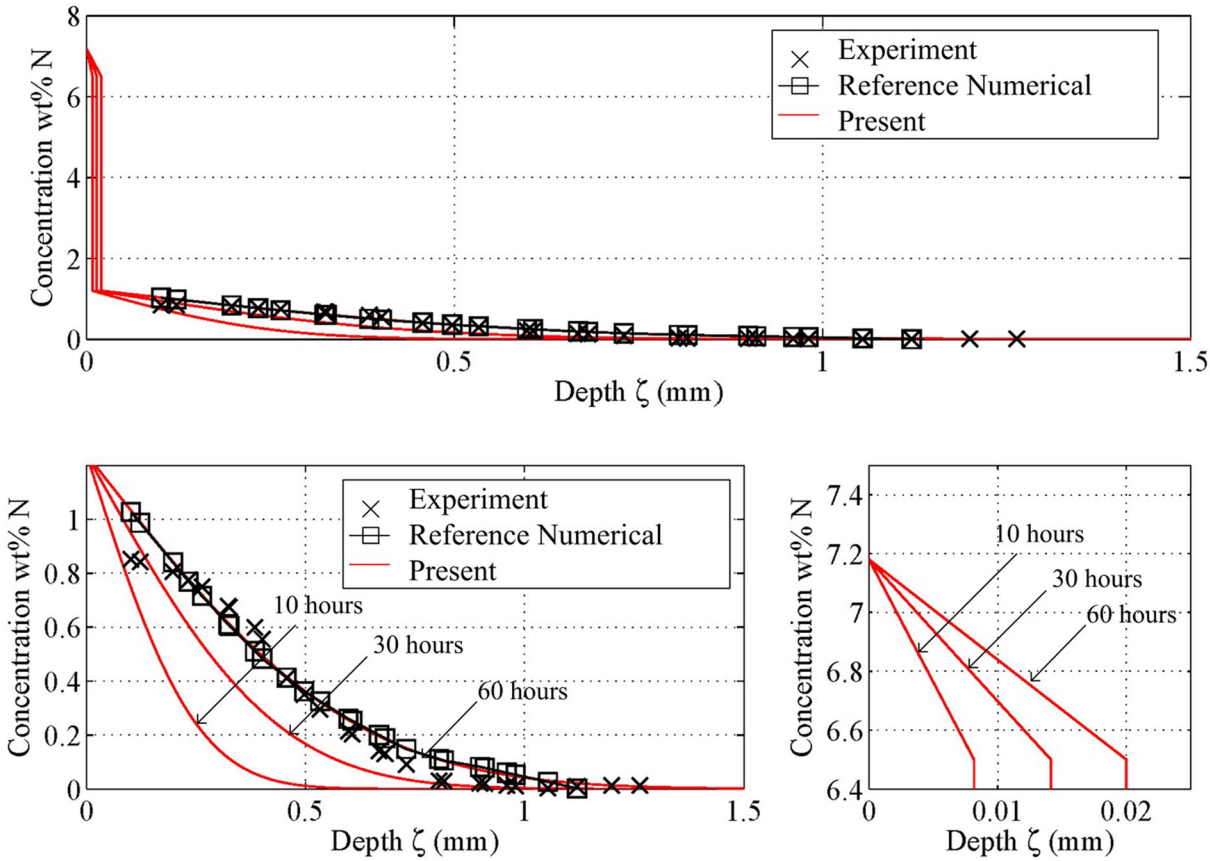

Fig. 2 Comparisons of nitrogen concentration profiles at different nitriding time in (top) the whole nitrided depth; (bottom left) in diffusion zone; (bottom right) in compound layer

$$v_{\Phi_i} = V_{\text{lattice}} \cdot A / \sum_{j=1}^{q} \left(N_{\Phi_i}^{Z_j} \cdot M^{Z_j} \right), \tag{Eq 6}$$

$$V_p = m \cdot \sum_{i=2}^{n} (v_{\Phi_i} \omega_{\Phi_i}). \tag{Eq 7}$$

Here, A is Avogadro's number. V_{lattice} is the elementary volume of phase Φ_i. $N_{\Phi}^{Z_j}$ is the stoichiometric coefficient of element Z_j in phase Φ_i. The molar weight of element Z_j is denoted by M^{Z_j}. m is the total mass of the system. ω_{Φ_i} is the weight fraction of phase Φ_i before nitriding. Assume the heavy elements p, such as Fe and Cr in AISI 4140 steel, do not diffuse during the nitriding process, and the quantities of the heavy elements are defined by ω^{Z_j} at time t and ω'^{Z_j} at time $t + \Delta t$. Moreover, due to the diffusion of nitrogen, the mass increase in the system between time t and $t + \Delta t$ is denoted by Δm. At time $t + \Delta t$, the volume of precipitates is changed to V_P'. The mass increase Δm and V_P' can then be calculated by

$$\Delta m = m \cdot \left(\sum_{j=1}^{p} \omega^{Z_j} \Big/ \sum_{j=1}^{p} \omega'^{Z_j} - 1 \right), \tag{Eq 8}$$

$$V_P = (m + \Delta m) \cdot \sum_{i=2}^{n} v_{\Phi_i} \cdot \omega'_{\Phi_i}. \tag{Eq 9}$$

Assume that the volume change in the matrix is negligible compared with precipitation, the volume change accompanying the precipitation can be written as follows (Ref 25)

$$\varepsilon_{ij}^{\text{vol}} = \frac{1}{3} \frac{\Delta V}{V} \delta_{ij} = y_P \cdot \frac{y'_P \cdot y_{Fe} - y_P \cdot y'_{Fe}}{y_p \cdot y'_{Fe}}, \tag{Eq 10}$$

where y_{Φ_i} and y'_{Φ_i} are the volume fraction V_{Φ_i}/V of the phase Φ_i at time t and $t + \Delta t$.

2.3 Solution Procedure of Residual Stress Using Finite Element Simulation

On the basis of the volume strain estimated above, the residual stresses and distortions can then be evaluated using finite element method by introducing the corresponding volumetric strain to each element. In order to produce the corresponding volumetric strain, the thermal expansion procedure in ABAQUS™ is a simple but effective way. We assume the whole body has the thermal expansion coefficient α, which is in the complete form (vector with all components, i.e., α_{11} and α_{12}). In a matter of fact, the thermal expansion coefficients in different phases are different. The thermal expansion coefficient is related to nitrogen concentration and the microstructures of different phases. However, due to the lack of the thermal expansion coefficient data of these different phases, we assumed that the thermal expansion coefficients are constant and the same to that of the base material AISI 4140

steel in the FEM analysis, i.e., α = 14.6E−6/°C. Based on this assumption, the structural dilation strain field can be introduced by the following method.

The initial non-physical temperature of the whole body is assumed to be T. If a non-physical temperature change field $\Delta T(\mathbf{x})$ is applied on the whole body, the thermal strain field will be $\varepsilon^{\text{vol}} = (1 + \alpha \cdot \Delta T(\mathbf{x}))^3 - 1$. In order to reproduce the volumetric strain field presented in Eq 10, the non-physical temperature change field can then be easily determined by

$$\Delta T(\mathbf{x}) = \left(\sqrt[3]{1 + \varepsilon^{\text{vol}}} - 1\right)/\alpha. \quad \text{(Eq 11)}$$

This temperature change field is applied on the nodes using user subroutine UTEMP in ABAQUS™. The estimated residual volume strain given in Eq 10 will be produced after performing thermal analysis with the non-physical temperature change field in Eq 11. The resultant residual volume strain will yield the distortion of the specimen and produce residual stresses, which will be shown later in this work and compared with experimental results.

The plastic strain is included by considering the plasticity of AISI 4140 steel. Comparing with the thickness of the diffusion region and the dimension of the whole component, the thickness of the compound layer is very thin. Therefore, in this research it is assumed that the influence of the plasticity of compound layer is marginal, and the residual stress in compound arises from the structural dilation and thermal residual strain. The plasticity behavior of the material is implemented by selecting proper material model in ABAQUS™.

The FEM analysis also considered thermal residual strains due to the temperature change in nitriding process. The steady-state thermal analysis for heating and cooling in nitriding is carried out, in which the sequential thermal-mechanical coupling FEM analysis has been employed.

The FEM analysis for nitriding includes the following three steps:

Step I The component is heating up from T_A = 27 °C to T_B = 527 °C.

Step II The non-physical temperature change field $\Delta T(\mathbf{x})$ calculated in Eq 11 is applied to the component, in order to introduce the volumetric strain due to the nitrogen diffusion. The temperature of the component is $T_C = T_B + \Delta T(\mathbf{x})$.

Step III The component is cooling down from T_C to $T_D = T_A + \Delta T(\mathbf{x})$.

In the FEM analysis procedure, the heating and cooling stages in Step I and Step III are assumed to be homogeneous in the component for the sake of simplicity.

The actual microstructure evolution is very complicated in compound layer and diffusion zone. The material properties in compound layer and diffusion zone are highly related to the concentration of nitrogen and other elements. The microstructures in the compound layer, diffusion zone, and base metal also significantly influence the material properties. In order to provide a macroscopic-scale FEM model for analyzing the residual stresses of real products in nitriding process, the materials are homogenized so that FE analysis becomes possible.

3. Residual Stress Measurement Using Micro-ring-Core Method

The AISI 4140 steel rod was machined into a 15-mm-diameter, 40-mm-long test sample. It was nitrided by using the industry two-stage gas nitriding process: The first stage was carried out using ammonia gas with dissociation rate of 24-28%

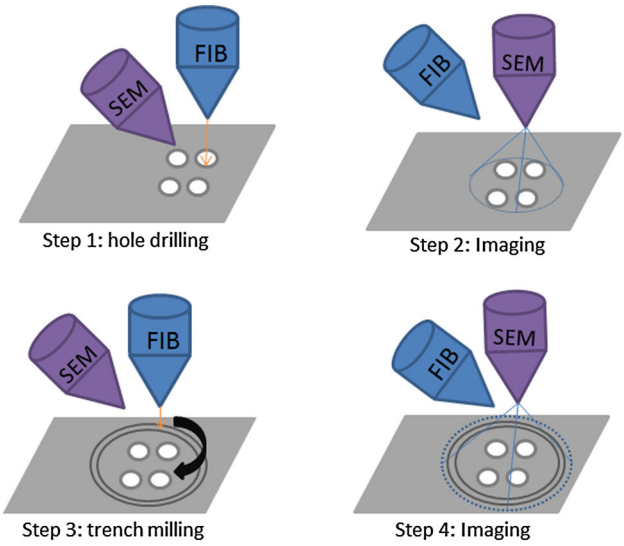

Fig. 4 Illustration of μRCM process steps

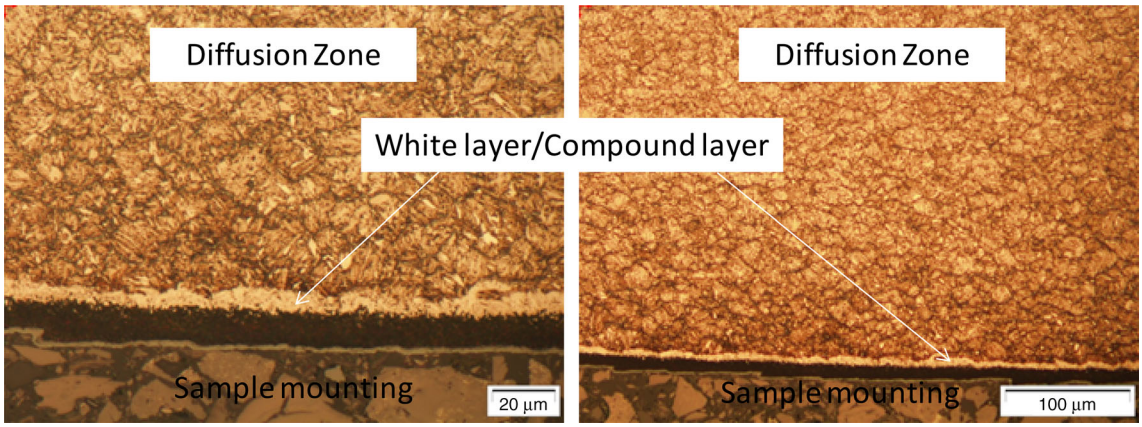

Fig. 3 Microstructure of AISI 4140 sample cross section: (a) is a magnification view of (b) to focus on the nitriding compound layer

at 527 °C for 10 h and the second stage was carried out using ammonia gas with dissociation rate of 79-82% for 50 h (Ref 7). Then, the sample was wire-cut and hot-mounted for further surface polishing. After polishing, 1% Nital etchant was used to reveal the microstructure. Figure 3 illustrates the AISI 4140 sample microstructure after nitriding, in which the nitriding white layer can be clearly observed.

The µRCM (micro-ring-core method) developed by Korsunsky et al. (Ref 13, 16, 17) was employed here to obtain the residual stresses at microscale. This method consists of FIB ring-core milling on the sample, high-resolution SEM imaging of the stress-relieved surface, a full-field strain analysis by digital image correlation (DIC) to obtain the strain change $\Delta\varepsilon$ and residual stress calculation based on Hooke's law for either equi-biaxial stress states or non-equi-biaxial stress states (Ref 13). For each µRCM measurement point, a 2×2 dotted pattern was firstly created by FIB, and then, the SEM was employed to take high-resolution image of the reference pattern with minimal beam damage to the surface. Subsequently, a circular trench (ring pattern) was cut around the pattern to fully release the strain at the surface to create an "island." The SEM micrograph of the patterned area on the "island" was again acquired at the same magnification and contrast after the milling step to compare with the initial one using DIC to obtain the relief strain value. Such µRCM step procedure is illustrated in Fig. 4. The desired ring-core pattern for current application is illustrated in Fig. 5(a). The white ring region represents the circular trench, which has 0.5 µm in width and 5 µm in depth. The inner big circle region represents the "island" with a diameter of 4.5 µm. The 2×2 dots matrix was patterned on top of it to facilitate the strain analysis by DIC as surface marking.

DIC analysis was carried out by a MATLAB®-based code using the correlation function *cpcorr*. Firstly, to facilitate the tracking process, SEM images taken before and after the ring milling were cropped to 290×290 pixels to focus on the 2×2 dots surface marking which provides the highest contrast. After that, a rectangular grid with 2 pixels spacing covering the patterned area was defined by the program (with MATLAB® functions filelist-generlator.m, grid_generator.m). Then, the displacements of all the dot array patterns under the inter

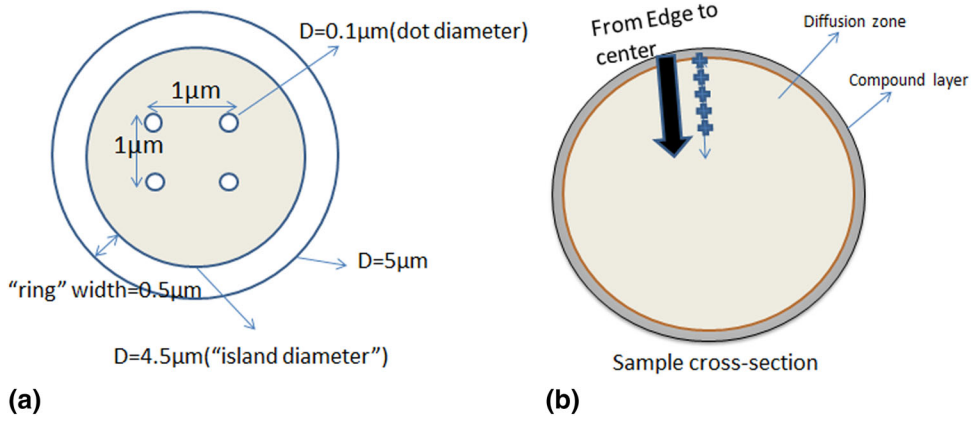

Fig. 5 (a). Regular hole patterning of 2×2 and circular island of diameter 4.5 µm; (b). location of patterns on cross-sectional area

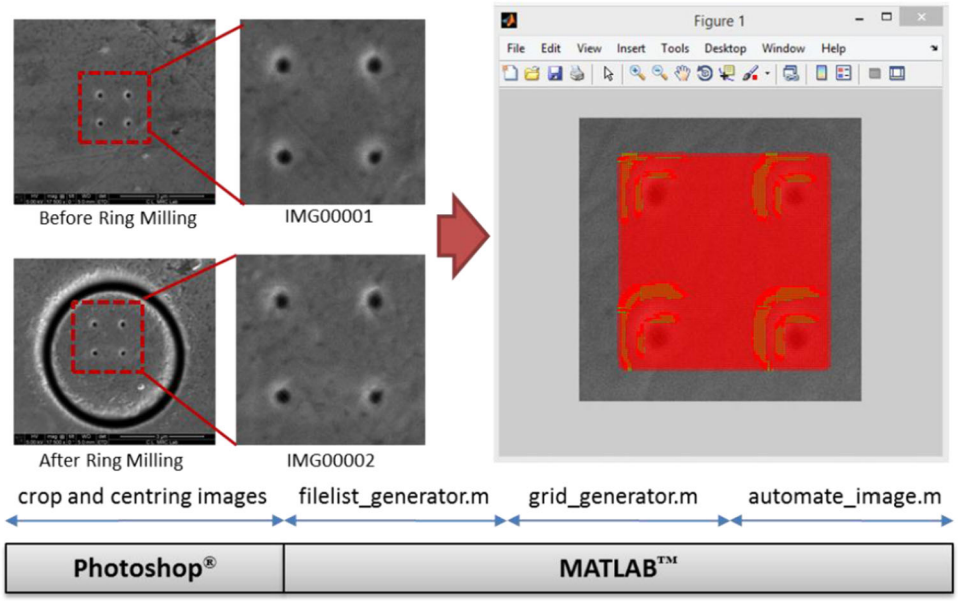

Fig. 6 Process of digital image correlation (DIC) for strain analysis utilizing the MATLAB functions

section of the grid were recognized and analyzed (MATLAB® function automate_image.m). In the end, strains of the areas covered by the grid were calculated by the program, and result is displayed (MATLAB® function displacement.m) (Fig. 6).

Starting from the edge of the sample, several rings were made along radius to the inner core to obtain the residual stresses profile against the nitriding depth, which is illustrated in Fig. 5(b). The locations of the rings are (from sample edge): 5, 10, 15 and 20 μm (compound layer); 30, 50, 100, 150, 200, 300, 400 and 500 μm (diffusion zone), respectively.

One of the biggest sources of error in this method is ion beam drifting. Such drift was corrected by creating a "cross-shaped" reference mark near pattern region(at a "safe" distance from island of interest) and using FIB to merely focus on the "cross" and measure the drifting distance with respect to the original coordination and make adjustment for trench milling (Ref 16). Figure 7 shows an example of the SEM image of two sacrificial markers (circled in red) together with ring and pattern. The "cross" mark here mainly serves for two functions: (1) monitoring the drifting of image when switching from SEM to FIB and helping with the targeting of trench milling process (drift correction) and (2) reducing pattern surface damage compared with direct imaging of pattern surface.

The milling speed of the ion beam also has to be studied before the actual μRCM to be carried out. The current milling speed is commonly calculated based on silicon samples. It needs to be converted to the sample material speed so that the depth of the milling can be obtained accurately to ensure that a full stress relief of the "island" can be achieved (condition: depth > diameter). Therefore, the milling speeds of AISI 4140 sample on both diffusion zone and compound layer were benchmarked against the silicon sample by milling a 3-μm-diameter shallow hole in 15 min. It was milled using a 30 keV 93 pA ion beam, which was also employed in our actual μRCM study. Result in Fig. 8(a) and (b) shows that the cutting speed of ion beam on silicon was approximately twice that of diffusion zone. As the ring depth should be greater than its diameter for a full strain relief, a >5-μm ring depth is required. Therefore, a milling depth (Si-equivalent) of at least 10 μm for diffusion zone is needed in the current study. We employed the same Si-equivalent milling depth for compound layer, which gives the actual depth ≈ 26 μm, also sufficient for the full stress relief condition to be met.

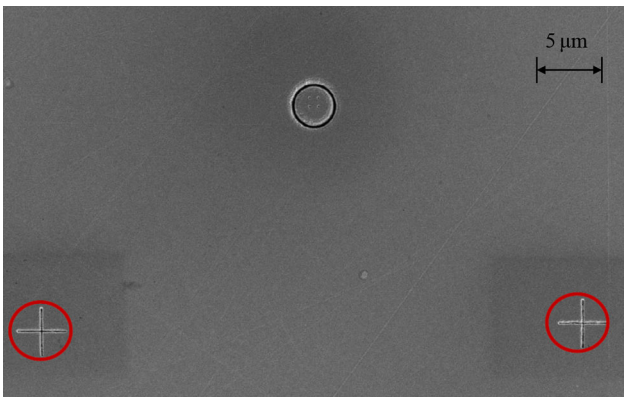

Fig. 7 SEM image of two sacrificial cross markers (circled) together with ring and pattern

4. Results and Discussion

4.1 Micro-hardness and SEM Micrograph

Micro-Vickers hardness tests have been carried out from the sample edge toward the core. Figure 9 illustrates the hardness depth profile of the nitrided sample. This also indicates that the nitriding case depth should be no more than 500 μm, which justifies the range of measurement points in the μRCM residual stresses study. The SEM image of the nitrided casing area is shown in Fig. 10, in which region A and region B represent the compound layer with relative darker color, and region C represents the diffusion zone region, where the color is lighter and more toward the inner surface. This is a classic three-layer nitriding case micrograph which can be observed in a similar study (Ref 26). To be more specific, Region A consists of two phases, γ'-Fe_4N (the light phase) and ε-$Fe_{2\text{-}3}(C, N)$ (the dark

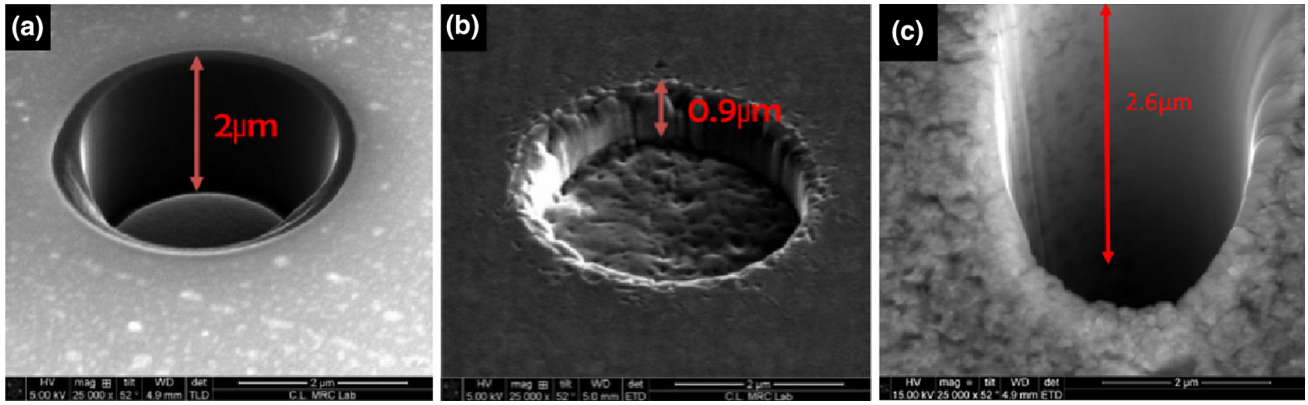

Fig. 8 FIB milling of a 3-μm-diameter hole on the sample of (a) silicon, (b) diffusion zone, (c) compound layer using identical ion beam milling parameters for depth benchmarking

phase). Region B is mainly dominated by γ'-Fe_4N, and in region C, martensite and Fe_3C are commonly found. From this image, the thickness of compound layer can be determined to be about 20 μm, which further justifies our μRCM measurement point selection. In this figure, an example of the micro-ring core (partial) and the "cross" reference can be seen.

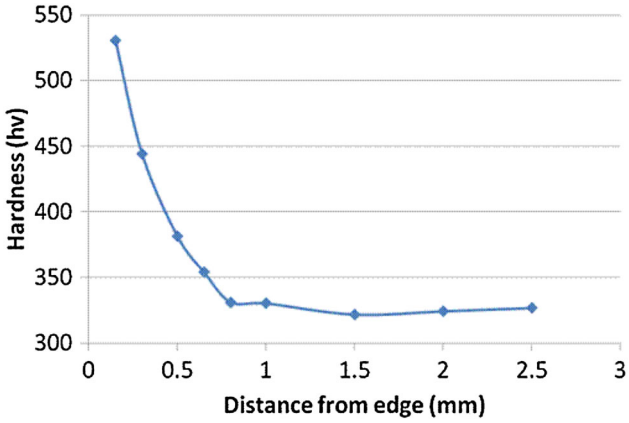

Fig. 9 Micro-hardness results in the nitrided samples

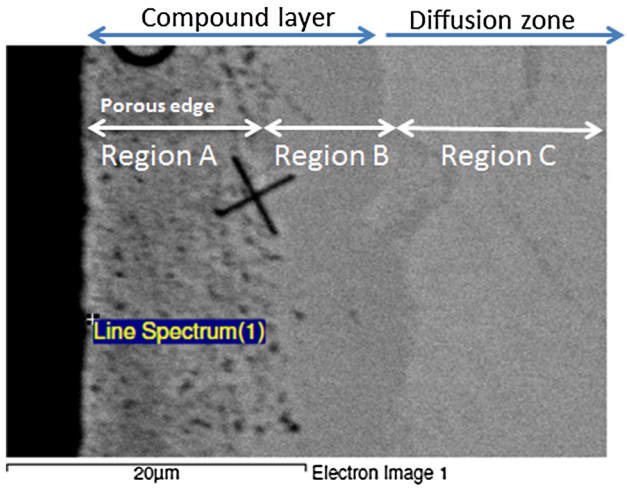

Fig. 10 SEM image of sample AISI 4140

4.2 Finite Element Simulation Result

An axisymmetric model was built to analyze the residual stresses and the distortion of a disk after nitriding, which is shown in Fig. 11. The dimensions of the disk are radius $r = 0.2$ m and thickness $h = 0.1$ m. 92,416 CAX4 elements are used to discretize the domain. The compound layer and diffusion zone are discretized using a very fine mesh, as shown in Fig. 11(b). The material properties used for simulation are listed in Table 1.

The residual stresses σ_{rr}, σ_{zz}, and $\sigma_{\theta\theta}$ after 60-h nitriding were evaluated. In order to compare the residual stresses with the experimental results, the residual stress component σ_{rr} along the disk center line was sampled and is plotted in Fig. 12. Compressive residual stresses were found in the compound layer and diffusion zone. Maximum compressive residual stress is around 800-900 MPa, which is in agreement with the experimental data. Figure 12 shows that in compound layer the residual stress profile shows a hump, not a monotonic variation. This phenomenon results from the discontinuous nitrogen concentration profile calculated in Eq 5 and the discontinuous misfit volume strain due to the discontinuous nitrogen concentration. As being calculated in section 2.2, the magnitude of volume strain in compound layer will degenerate to zero at the interface. The residual strain of the diffusion zone at the interface is not zero according to the modeling in section 2.3. However, in macroscopic-scale FEM simulation the steel specimen is a continuum body, and therefore, the interactions

Table 1 Material properties of AISI 4140 steel and Fe4N (27)

	Modulus of elasticity, GPa	Poisson's ratio	Tensile strength (yield), MPa	Tensile strength (ultimate), MPa
AISI 4140	205	0.29	800	965
Fe4N	160	0.36	…	…

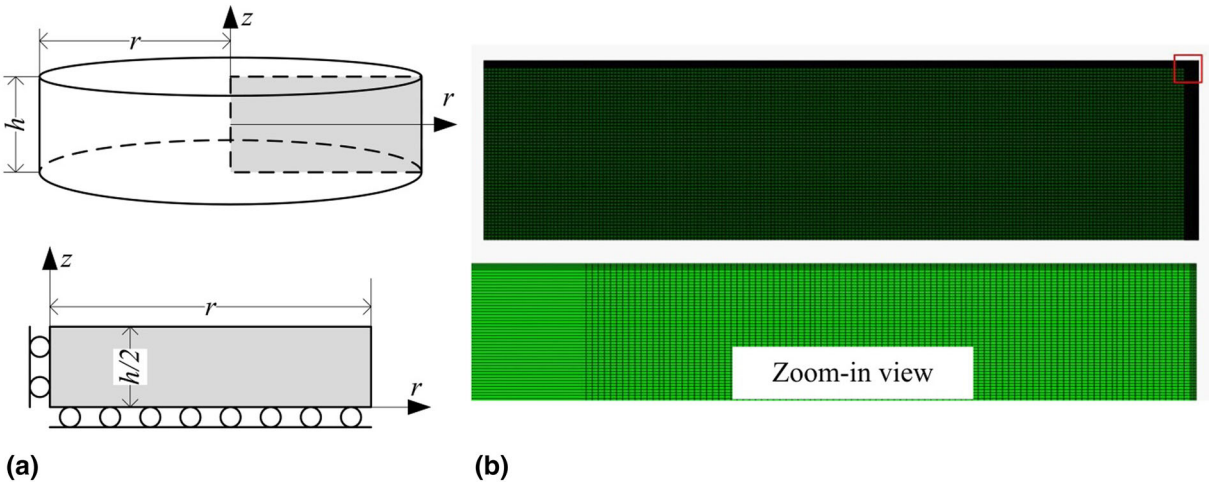

Fig. 11 (a) Computational model of an AISI 4140 steel disk for nitriding; (b) finite element mesh used for residual stress analysis

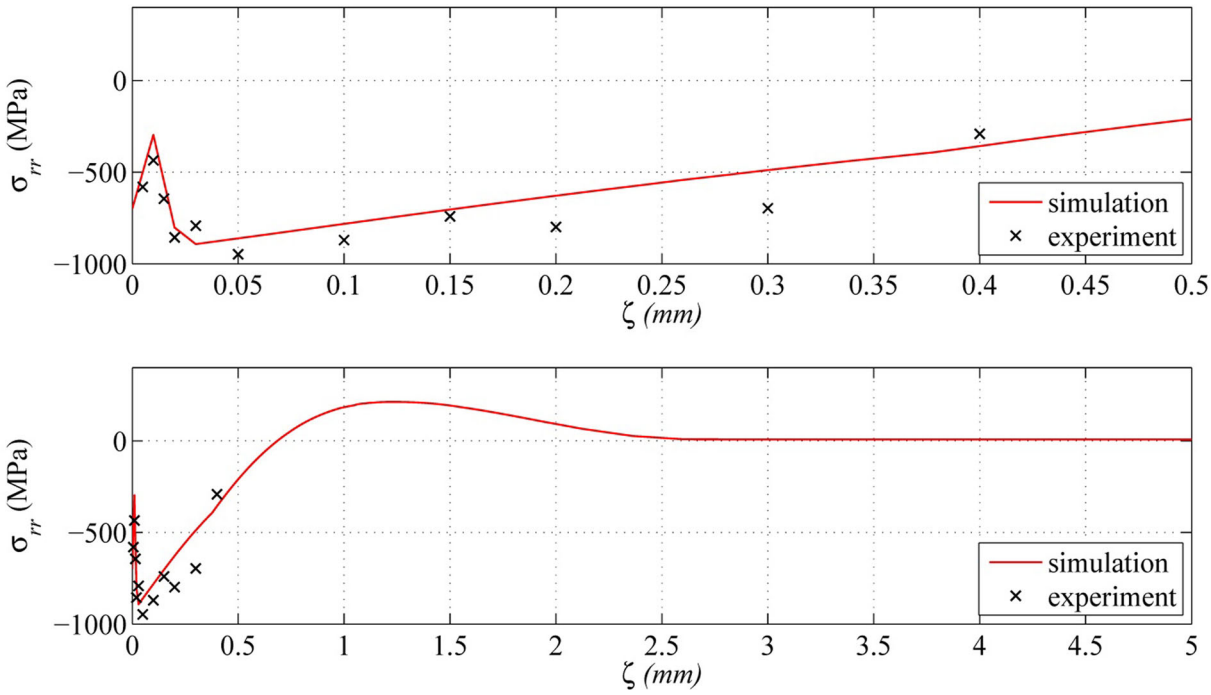

Fig. 12 Comparisons of residual stresses profiles obtained by finite element simulation and experiment using μRCM method

between diffusion zone and compound layer will influence the final deformation and the total residual stress distribution. The magnitude of the compressive residual stress in compound layer first decreases to a nonzero level at a certain depth and increases due to the influences of the diffusion zone. Because the compound layer is very thin, the influence from diffusion zone on the residual stress is significant and shows a sharp change. The compound layer also shows similar influence to the residual stress distribution in the diffusion zone, which makes the residual stress not changing monotonically, especially in the vicinity of the interface. In Fig. 12, one can also find that the residual stress becomes tensile stress in the region beyond the diffusion zone, which has also been found in the simulation and experimental results reported in the literature (Ref 25).

A good agreement of the numerical simulation results and the experimental data is shown in Fig. 12, which successfully validated both the experimental and numerical methodology in measuring and predicting the residual stress and distortion of AISI 4140 steel specimen after nitriding.

5. Conclusions

In the present study, the residual stresses distribution in the gas nitrided AISI 4140 sample has been obtained using both FE simulation and μRCM measurement, which allows obtaining the residual stress values in both the compound and diffusion layer with high resolution. A FEM model is proposed to analyze the residual stresses including plasticity, thermal, and structural dilation in nitriding process of AISI 4140 steel. Such model integrates existing diffusion model into the thermal-mechanical model so that the distortion in nitriding steel can be easily and readily obtained. More importantly, using this well-established model, we can provide theoretical explanation to the big stress variation we observed in the compound layer. Such variation is rarely reported previously due to the measurement resolution limit. Now we are using the novel μRCM to drive down the resolution, so that the residual stress variation at microscale level can be directly observed and explained.

References

1. C. Bever, Case Hardening of Steel by Nitriding, *surface protection Against Wear and Corrosion*, H.S. Avery, Ed., ASM International, Ohio, 1954, p 531–548
2. J.L. Dossett, G.E. Totten, Steel Heat Treating Fundamentals and Processes, ASM Handbook, Vol 4A, ASM International, Ohio, 2013
3. E.J. Mittemeijer and M.A.J. Somers, Thermodynamics, Kinetics, and Process Control of Nitriding, *Surf. Eng.*, 1997, **13**, p 483–497
4. M. Yang, Nitriding-Fundamentals, Modelling and Process Optimization, PhD thesis, Worcester Polytechnic Institute, MA, April 2012
5. M.A.J. Somers and E.J. Mittemeijer, Layer-Growth Kinetics on Gaseous Nitriding of Pure Iron—Evaluation of Diffusion-Coefficients for Nitrogen in Iron Nitrides, *Metall. Mater. Trans. A*, 1995, **26**, p 57–66
6. L. Torchane, P. Bilger, J. Dulcy, and M. Gantois, Control of Iron Nitride Layers Growth Kinetics in the Binary Fe–N System, *Metall. Mater. Trans. A*, 1996, **27**, p 1823–1835
7. M. Yang and R.D. Sisson, Jr., Modeling the Nitriding Process of Steels, *Adv. Mater. Proc.*, 2012, **170**, p 33–36
8. G. Totten, Residual Stress in Nitriding, in: Handbook Of Residual Stress and Deformation of Steel, ASM International, Ohio, 2002, p. 210–218
9. F.T. Hoffman, U. Kreft, T. Hirsch, and P. Mayr, In situ measurement of residual stresses during the nitriding process, *Proceeding of the second international conference of carburizing and nitriding with atmospheres*, ASM International, Cleveland, OH, 1995, p 289–293
10. X. Song, W.C. Liu, J.P. Belnoue, J. Dong, G.H. Wu, W.J. Ding, S.A.J. Kimber, T. Buslaps, A. Lunt, and A.M. Korsunsky, An Eigenstrain-Based Finite Element Model and the Evolution of Shot Peening Residual Stresses During Fatigue of GW103 Magnesium Alloy, *Int. J. Fatigue*, 2012, **42**, p 284–295

11. S.S. Akhtar, A.F.M. Arif, and B.S. Yilbas, Influence of Multiple Nitriding on the Case Hardening of H13 Tool Steel: Experimental and Numerical Investigation, *Int. J. Adv. Manuf. Technol.*, 2012, **58**, p 57–70
12. F. Vaz, L. Rebouta, Ph Goudeau, J.P. Riviere, E. Schaffer, G. Kleer, and M. Bodmann, Residual Stress States in Sputtered $Ti_{1-x}Si_xN_y$ Films, *Thin Solid Films*, 2002, **402**, p 195–202
13. A.M. Korsunsky, M. Sebastiani, and E. Bemporad, Focused Ion Beam Ring Drilling for Residual Stress Evaluation, *Mater. Lett.*, 2009, **63**, p 1961–1963
14. P.J. Withers and H.K.D.H. Bhadeshia, Residual Stress Part 1—Measurement Techniques, *Mater. Sci. Technol.*, 2001, **17**, p 355–365
15. A.M. Korsunsky, S. Cherian, R. Raiteri, and R. Berger, On the Micromechanics of Micro-cantilever Sensors: Property Analysis and Eigenstrain Modeling, *Sens. Actuators, A*, 2007, **139**, p 70–77
16. A.M. Korsunsky, M. Sebastiani, and E. Bemporad, Residual Stress Evaluation at the Micrometer Scale: Analysis of Thin Coatings by FIB Milling and Digital Image Correlation, *Surf. Coat. Technol.*, 2010, **205**, p 2393–2403
17. M. Sebastiani, C. Eberl, E. Bemporad, A.M. Korsunsky, W.D. Nix, and F. Carassiti, Focused Ion Beam Four-Slot Milling for Poisson's Ratio and Residual Stress Evaluation at the Micron Scale, *Surf. Coat. Technol.*, 2014, **251**, p 151–161
18. K.J. Kang, N. Yao, M.Y. He, and A.G. Evans, A Method for in Situ Measurement of the Residual Stress in Thin Films by Using the Focused Ion Beam, *Thin Solid Films*, 2003, **443**, p 71–77
19. M. Krottenthaler, C. Schmid, J. Schaufler, K. Durst, and M. Göken, A Simple Method for Residual Stress Measurements in Thin Films by Means of Focused Ion Beam Milling and Digital Image Correlation, *Surf. Coat. Technol.*, 2013, **215**, p 247–252
20. X. Song, K.B. Yeap, J. Zhu, J. Belnoue, M. Sebastiani, E. Bemporad, K.Y. Zeng, and A.M. Korsunsky, Residual Stress Measurement in Thin Films at Sub-micron Scale Using Focused Ion Beam Milling and Imaging, *Thin Solid Films*, 2012, **520**, p 2073–2076
21. E.A. Ochoa, C.A. Figueroa, and F. Alvarez, Nitriding of AISI, 4140 Steel by a Low Energy Broad Ion Source, *J. Vac. Sci. Technol. A*, 2006, **24**, p 2113–2116
22. J. Crank, *The Mathematics of Diffusion*, 2nd ed., Oxford University Press, London, 1975
23. Barrallier L, Barralis J. On origin of residual stresses generated by nitriding treatment on alloy steels, *Proceedings of ICRS4*. Baltimore, (MD), Society for Experimental Mechanics Inc. USA, 1994, p 498–505
24. S. Jegou, R. Kubler, and L. Barrallier, On Residual Stresses Development during Nitriding of Steel: Thermochemical and Time Dependence, *Adv. Mater. Res.*, 2010, **89**, p 256–261
25. S. Jegou, L. Barrallier, and R. Kubler, Phase Transformations and Induced Volume Changes in a Nitrided Ternary Fe–3%Cr–0.345%C Alloy, *Acta Mater.*, 2010, **58**, p 2666–2676
26. M. Yang, B. Bao, Y.H. Sohn, and R.D. Sisson, Jr., Simulation of the Ferritic Nitriding Process, *Int. Heat Treat. Surface Eng.*, 2011, **5**, p 122–126
27. T. Takahashi, J. Burghaus, D. Music, R. Dronskowski, and J.M. Schneider, Elastic Properties of γ'-Fe_4N probed by Nanoindentation and Ab Initio Calculation, *Acta Mater.*, 2012, **60**, p 2054–2060